

Efficient Time-domain Sensitivity Analysis using Coarse Grids

Y. Song, N. K. Nikolova, and M. H. Bakr

Department of Electrical and Computer Engineering
McMaster University, Hamilton, ON L8S 4K1, Canada

songyp@grads.ece.mcmaster.ca, talia@mail.ece.mcmaster.ca, mbakr@mail.ece.mcmaster.ca

Abstract — We propose an efficient coarse-grid approach to the sensitivity analysis with full-wave electromagnetic (EM) time-domain simulations. In order to compute the response sensitivity using an adjoint approach, waveforms at all perturbation grid points need to be saved and post-processed. Therefore, the memory requirements of the response sensitivity analysis may become excessive for electrically large objects or problems with a large number of optimizable parameters. The use of coarse grids can reduce these memory requirements drastically and improve the computational efficiency of the sensitivity analysis while maintaining good accuracy. In this paper, we show that the discretization step size used in the sensitivity computation can be many times larger than the step size used in the finite-difference time-domain (FDTD) simulation. The effects of the coarseness of the grid on the accuracy of the sensitivity analysis are investigated. Verification is carried out through 1-D, 2-D and 3-D lossy dielectric structures using commercial FDTD solvers.

Keywords: Time-domain analysis, sensitivity analysis, Jacobian computation, and adjoint-variable method.

I. INTRODUCTION

The sensitivity analysis of microwave problems is important in gradient-based computer-aided design [1-4] and inverse-problem solutions [5]. It yields the response gradients (Jacobians) with respect to the optimizable shape and material parameters. Jacobians are widely used for efficient optimization, modeling, tolerance and yield analyses.

Jacobians are usually computed using response-level finite differences (FDs). For a problem with n design parameters, such an approach requires n additional simulations if forward or backward differences are used. The optimization cycle can easily become prohibitively slow due to the computational demand of the full-wave simulations. Beside its inefficiency, it is also shown in [6]

to [7] that the FD approaches are unreliable, i.e. they may be prone to numerical noise [6].

In contrast, the Jacobian computation using adjoint-based methods is efficient and reliable. Over the last several years, the adjoint variable method has been studied extensively in the sensitivity analysis of transient electromagnetic (EM) systems. An adjoint approach needs at most two system analyses to compute the response Jacobians regardless of the number of the optimizable parameters. In [1-3], Chung *et al.* have proposed an exact adjoint-variable expression for high-frequency problems. This exact approach is only applicable to unstructured-grid solvers since analytical system matrix derivatives are needed. Later, Nikolova *et al.* [8] and Bakr and Nikolova [9] proposed a new adjoint-based time-domain approach based on finite-difference time-domain (FDTD) and transmission-line matrix simulations. A discrete sensitivity expression of second-order accuracy is derived based on the \mathbf{E} -field vector wave equation [8]. This approach does not need analytical system matrix derivatives and allows sensitivity computation on structured grids.

Recently, we proposed a self-adjoint approach to compute responses, such as network parameters or point-wise response functions, and their Jacobian matrices use only one EM system analysis [7, 10-11]. Our approach is efficient, accurate and versatile. The adjoint field solution is obtained directly from the original field solution by some simple mathematical transformations. Adjoint simulations are not needed. Thus, this self-adjoint formulation reduces in half the computational cost in comparison with the existing adjoint methods [1-3] and [8-9]. More importantly, it is applicable with commercial EM solvers, since the Jacobian computation is reduced to a post-process of the EM field solution. In contrast, currently existing adjoint approaches [1-3] and [8-9] are only applicable to in-house codes. This is because the excitation distribution of the adjoint simulations is response dependent, which is difficult to set up in a commercial solver.

In our original self-adjoint approach, the sensitivity solver adopts the grid of the FDTD simulation for the computation of the response gradient. For this computation, at each perturbation grid point, the waveforms of all three \mathbf{E} -field components need to be stored. However, this may increase the memory requirements, especially in the case of electrically large regions whose permittivity or conductivity distribution is being optimized. For some time-domain solvers, the speed of the overall simulation may be affected as well. This happens if the simulator stores on the hard disk the requested \mathbf{E} -field solution at each iteration [12]. Slow-down due to recording the field solution is insignificant if the latter is exported after the simulation is over [13]. Even in this case, when the time-domain simulation is very long and the number of required field points is large, the memory requirements may become excessive.

In order to alleviate the problems described above, we propose the use of an independent coarse FD grid for the sensitivity analysis. We show that this grid can be many times coarser than the one used in the FDTD simulation. Recommendations are given for a proper choice of its step size.

We start with a brief overview of the time-domain self-adjoint sensitivity analysis. Then, we describe the implementation of the coarse-grid in inhomogeneous structures containing lossy dielectric objects. We investigate the accuracy of the proposed coarse grid approach through 1-D, 2-D and 3-D examples.

II. BACKGROUND

A. Self-adjoint S-parameter Sensitivities

The S-parameters of a multi-port structure can be expressed as [7],

$$S_{pq}^{\omega_0} = \sqrt{\frac{Z_q^{\omega_0}}{Z_p^{\omega_0}}} \cdot \frac{\tilde{F}_{pq}^{\omega_0}}{\tilde{F}_q^{\omega_0}} \quad (1)$$

where

$$\tilde{F}_{pq}^{\omega_0} = \int_0^{T_{\max}} \iint_{S_{p\text{-port}}} \mathbf{E}_q^{\text{out}}(x'_p, y'_p, t) \cdot \mathbf{M}_p(x'_p, y'_p) dx'_p dy'_p \cdot e^{-j\omega_0 t} dt, \quad (2)$$

$$\tilde{F}_q^{\omega_0} = \int_0^{T_{\max}} \iint_{S_{q\text{-port}}} \mathbf{E}_q^{\text{in}}(x'_q, y'_q, t) \cdot \mathbf{M}_q(x'_q, y'_q) dx'_q dy'_q \cdot e^{-j\omega_0 t} dt. \quad (3)$$

Here, T_{\max} is the simulation time; the subscript q in \mathbf{E}_q denotes the field solution when port q is excited, and the superscripts *out* and *in* denote the outgoing (scattered)

and incoming (incident) wave, respectively; \mathbf{M}_ξ ($\xi = p, q$) is the field modal (orthonormal) vector at port ξ [14]; x'_ξ and y'_ξ ($\xi = p, q$) are the coordinates at the ξ^{th} port plane; $Z_\xi^{\omega_0}$ ($\xi = p, q$) is the wave impedance of the ξ^{th} port; and ω_0 is the frequency at which the S-parameters are computed. For brevity, the superscript ω_0 will be omitted but implied in all formulas hereafter.

Consider a set of N optimizable parameters p_n , $n = 1, \dots, N$, which represent the shape and constitutive parameters of the structure. Assuming that the parameter changes do not affect the port waveguides, the derivative of the S-parameter with respect to p_n is,

$$\frac{\partial S_{pq}}{\partial p_n} = \sqrt{\frac{Z_q}{Z_p}} \cdot \frac{1}{\tilde{F}_q} \cdot \frac{\partial \tilde{F}_{pq}}{\partial p_n}, \quad n = 1, \dots, N. \quad (4)$$

The complex response \tilde{F}_{pq} whose derivative is needed in equation (4) allows for a self-adjoint formulation of the sensitivity problem. This means that the associated adjoint-field solutions $(\hat{\mathbf{E}}_p)_R$ and $(\hat{\mathbf{E}}_p)_I$ [9] can be obtained from the original-field solution \mathbf{E}_p where port p is excited. Here, $(\hat{\mathbf{E}}_p)_R$ and $(\hat{\mathbf{E}}_p)_I$ are the adjoint fields needed to compute the real and imaginary parts of $\partial \tilde{F}_{pq} / \partial p_n$, respectively. Thus, in our self-adjoint formulation, adjoint simulations are not needed. The computation of $(\hat{\mathbf{E}}_p)_R$ and $(\hat{\mathbf{E}}_p)_I$ from \mathbf{E}_p is briefly explained below.

The adjoint current density $\hat{\mathbf{J}}_{pq}$ is the derivative of the local response $f(\mathbf{E}, \mathbf{p})$ with respect to the field \mathbf{E} at the p^{th} port [8]. Its distribution across the port is the same as that of the current density \mathbf{J} . In the case of the S_{pq} derivatives, the real and imaginary parts of $\hat{\mathbf{J}}_{pq}$ are [7],

$$(-\hat{\mathbf{J}}_{pq})_R(x'_p, y'_p, t) = \mathbf{M}_{p\perp}(x'_p, y'_p) \cdot \hat{g}_R^{\omega_0}(t) \quad (5)$$

$$(-\hat{\mathbf{J}}_{pq})_I(x'_p, y'_p, t) = \mathbf{M}_{p\perp}(x'_p, y'_p) \cdot \hat{g}_I^{\omega_0}(t), \quad (6)$$

where

$$\hat{g}_R^{\omega_0}(t) = \frac{\sin(\omega_0 t)}{\omega_0 \beta \Delta t \Delta z_p}, \quad \hat{g}_I^{\omega_0}(t) = \frac{\cos(\omega_0 t)}{\omega_0 \beta \Delta t \Delta z_p}. \quad (7)$$

When the adjoint problem is excited by $-\hat{\mathbf{J}}_{pq}$ and runs backwards in time, i.e. $\tau = T_{\max} - t$, it is equivalent to the original problem [8]. To make the adjoint simulation in the backward running τ -time identical to the original one in forward t -time, we assume that the adjoint problem is excited by the reversed pulse $\hat{g}(\tau) = g(t)$, where $g(t)$ is the time waveform of the original excitation. The ω_0 spectral component of $\hat{g}(t)$ is related to that of $g(t)$ as [7],

$$\hat{g}^{\omega_0}(t) = G_m \cos(\omega_0 t - \varphi_g - \omega_0 T_{\max}) \quad (8)$$

where G_m and φ_g are the magnitude and phase of the ω_0 spectral component of $g(t)$. Due to the equivalence between the original and the backward-running adjoint problem, the adjoint field is related to the original one at a point P as,

$$\hat{\mathbf{E}}_p(P, T_{\max} - t) = \mathbf{E}_p(P, t) \quad (9)$$

and its ω_0 spectral component is

$$\hat{E}_{\zeta p}^{\omega_0}(P, t) = |E_{\zeta p}^{\omega_0}| \cos(\omega_0 t - \varphi_{e\zeta p(P)} - \omega_0 T_{\max}), \quad \zeta = x, y, z. \quad (10)$$

Here, ζ denotes the vector component; $|E_{\zeta p}^{\omega_0}|$ and $\varphi_{e\zeta p(P)}$ are the magnitude and the phase of the ω_0 spectral component of the original $E_{\zeta p}$ waveform at P .

By comparing the desired adjoint excitation waveform in equation (7) with that in equation (8), the adjoint field of equation (10) should be adjusted both in magnitude and phase in order to obtain $(\hat{\mathbf{E}}_p)_R$ and $(\hat{\mathbf{E}}_p)_I$ as [7],

$$\begin{aligned} (\hat{E}_{\zeta p}^{\omega_0})_R(P, t) = & \\ \frac{|E_{\zeta p}^{\omega_0}|}{J_{0p} G_m \omega_0 \beta \Delta t \Delta z} \cos(\omega_0 t - \varphi_{e\zeta p(P)} + \varphi_g - \pi/2) & \quad (11) \end{aligned}$$

$$\begin{aligned} (\hat{E}_{\zeta p}^{\omega_0})_I(P, t) = & \\ \frac{|E_{\zeta p}^{\omega_0}|}{J_{0p} G_m \omega_0 \beta \Delta t \Delta z} \cos(\omega_0 t - \varphi_{e\zeta p(P)} + \varphi_g), \quad \zeta = x, y, z. & \quad (12) \end{aligned}$$

Here, G_m and φ_g are the magnitude and phase of the ω_0 spectral component of the original excitation waveform $g(t)$; $|E_{\zeta p}^{\omega_0}|$ and $\varphi_{e\zeta p(P)}$ are the magnitude and phase of the ω_0 spectral component of the ζ -component of the original \mathbf{E} -field at point P ; Δz is the longitudinal cell size at the port; Δt is the discretization step in time; β is a constant defined as $\beta = \mu_0 \Delta h^2 / \Delta t$, where $\Delta h = \min(\Delta x, \Delta y, \Delta z)$; J_{0p} is the scaling factor determining the strength of the original excitation (usually set to 1).

B. Sensitivity of a Response at a Point

In open problems with a point excitation at point Q and a field observation at point P , there are no waveguide ports and the definition in equation (1) is simplified as follows: (i) the modal wave impedances are replaced by the intrinsic impedances Z_p and Z_Q of the media at which point P and point Q are located; (ii) the incoming phasor \tilde{F}_q is replaced by the ω_0 spectral component \tilde{E}_Q of the incident field $E_Q(t)$ at point Q , (iii) the outgoing phasor \tilde{F}_{pq} is replaced by the ω_0 spectral component \tilde{E}_{PQ} of the observed scattered field $E_{PQ}(t)$ at P . The

response then becomes,

$$F_{PQ} = \sqrt{\frac{Z_Q}{Z_P}} \cdot \frac{\tilde{E}_{PQ}}{\tilde{E}_Q}. \quad (13)$$

Here, the scalar scattered field response \tilde{E}_{PQ} and the incident field response \tilde{E}_Q are defined as,

$$\tilde{E}_{PQ} = \tilde{\mathbf{E}}_{PQ} \cdot \tilde{\mathbf{M}}_P \quad (14)$$

$$\tilde{E}_Q = \tilde{\mathbf{E}}_Q \cdot \tilde{\mathbf{M}}_Q, \quad (15)$$

where $\tilde{\mathbf{E}}_{PQ}$ is the ω_0 spectral component of the scattered vector field $\mathbf{E}_{PQ}(t)$ at point P when point Q is excited and $\tilde{\mathbf{E}}_Q$ is the ω_0 spectral component of the incident vector field $\mathbf{E}_Q(t)$ at point Q when point Q is excited. $\mathbf{E}_Q(t)$ is obtained through a reference simulation where point Q is excited in an infinite uniform medium of the same electrical properties as the medium at point Q and the field $\mathbf{E}_Q(t)$ is recorded at the point of excitation. $\tilde{\mathbf{M}}_\xi$ ($\xi = P, Q$) is the desired polarization vector [14] at point ξ , which is a complex vector in general.

The derivative of F_{PQ} with respect to the n th parameter can be expressed as,

$$\frac{\partial F_{PQ}}{\partial p_n} = \sqrt{\frac{Z_Q}{Z_P}} \cdot \frac{1}{\tilde{E}_Q} \cdot \frac{\partial \tilde{E}_{PQ}}{\partial p_n} \quad (16)$$

where the derivative of \tilde{E}_{PQ} is computed as that of \tilde{F}_{pq} in the case of the S -parameters. The adjoint fields are derived as before.

C. Sensitivity Formula

The conventional sensitivity expressions rely on analytical derivatives of the system coefficients, i.e., the coefficients of the governing equations, with regard to the parameter of interest p_n . However, on structured grids, as those used by finite-difference methods or transmission-line methods, the system coefficients are not analytical functions of the structure's shape parameters. Consequently, their derivatives are not available analytically. To deal with such cases, a second-order accurate sensitivity formula was proposed in [8-9], which is specifically developed for discrete parameter spaces. It allows the use of a stepwise perturbation of a shape parameter equal to that of the local cell size Δh , i.e. $\Delta p_n = \pm \Delta h$. Such a perturbation results in well defined changes in the system coefficients, which yield accurate results when used in the discrete sensitivity formula. Later, we discuss the possibility of using much larger cell sizes, which are multiples of Δh .

In the case of the complex response \tilde{F}_{pq} in equation (4), the discrete sensitivity formula for the real and imaginary parts of its derivative is [7],

$$\left(\frac{\partial \tilde{F}_{pq}}{\partial p_n} \right)_{R,I} \approx \int_0^{T_{\max}} \iiint_{\Omega} (\hat{\mathbf{E}}_p)_{nR,I} \cdot \frac{\Delta_n R(\mathbf{E}_q)}{\Delta p_n} d\Omega dt, \quad n=1, \dots, N \quad (17)$$

where

$$\begin{aligned} \frac{\Delta_n R(\mathbf{E}_q)}{\Delta p_n} &= \frac{\Delta_n \mathcal{C}^2}{\Delta p_n} \mathbf{E}_q - \frac{\Delta_n \alpha}{\Delta p_n} \cdot D_{ii} \mathbf{E}_q \\ &\quad - \frac{\Delta_n s}{\Delta p_n} \cdot D_{i2} \mathbf{E}_q - \frac{\Delta_n (\beta D_t \mathbf{J})}{\Delta p_n}. \end{aligned} \quad (18)$$

Here, the subscripts R and I denote the real and the imaginary part of a complex quantity, respectively, and Δ_n denotes a stepwise change occurring in a system coefficient as a result of the perturbation Δp_n of the n th parameter; Ω is the computational volume; \mathbf{E}_q is the original field solution of the nominal structure when port q is excited, and $(\hat{\mathbf{E}}_p)_{nR,I}$ are the field solutions of the adjoint problems in the n th perturbed state when port p is excited. Note that the adjoint field solutions for the real and the imaginary parts of the complex derivative are different and obtained from the original field solution \mathbf{E}_p (when port p is excited) using equations (11) and (12). Note also that the adjoint solutions must correspond to the n th perturbed state, i.e. the structure where p_n is perturbed by the smallest on-grid perturbations. However, no actual simulations of the perturbed structures are performed since their respective field solutions are approximated by a simple mapping procedure [8], which involves a one-cell shift in the direction of the respective perturbations. These approximations use the available field solution of the unperturbed structure only.

With a further regard to equation (18), the system coefficients α , β and s are,

$$\alpha = \varepsilon_r \left(\frac{\Delta h}{c\Delta t} \right)^2, \quad \beta = \mu_0 \frac{\Delta h^2}{\Delta t}, \quad s = \frac{\sigma \mu_0 \Delta h^2}{2\Delta t}. \quad (19)$$

They correspond to a central finite-difference discretization of the \mathbf{E} -field vector wave equation. The operators D_{ii} , D_{i2} and D_t are respective second- and first-order finite-difference operators with respect to time. \mathcal{C}^2 is the FD double-curl operator of the \mathbf{E} -field vector wave equation. Points, at which the expression (18) is non-zero, are referred to as perturbation grid points.

In the case when the optimizable parameter p_n is a material parameter, the derivatives of the system coefficients can be computed analytically. Also, $\Delta_n \mathcal{C}^2$

and $\Delta_n (\beta D_t \mathbf{J})$ in equation (18) are equal to zero since the system coefficients \mathcal{C}^2 and $\beta D_t \mathbf{J}$ are independent of variations in the material parameters in the case of dielectric structures. Thus, equation (18) can be written in an analytical form as,

$$\frac{dR(\mathbf{E}_q)}{dp_n} = -\frac{d\alpha}{dp_n} \cdot D_{ii} \mathbf{E}_q - \frac{ds}{dp_n} \cdot D_{i2} \mathbf{E}_q \quad (20)$$

where

$$\frac{d\alpha}{dp_n} = \begin{cases} \left(\frac{\Delta h}{c\Delta t} \right)^2, & p_n = \varepsilon_r \\ 0, & p_n = \sigma \end{cases} \quad (21)$$

$$\frac{ds}{dp_n} = \begin{cases} 0, & p_n = \varepsilon_r \\ \frac{\mu_0 \Delta h^2}{2\Delta t}, & p_n = \sigma. \end{cases} \quad (22)$$

Also, in this case, there is no need for the mapping approximation of the adjoint fields. The adjoint solutions correspond to the unperturbed structure and $(\hat{\mathbf{E}}_p)_{nR,I}$ in equation (17) are replaced simply by $(\hat{\mathbf{E}}_p)_{R,I}$.

Further details of the self-adjoint sensitivity computations are given in [11] with regard to acquiring the excitation waveform, the incident-field waveform, and the de-embedding required in the case of S -parameter sensitivities.

III. SENSITIVITY SOLVER GRID

In our discrete self-adjoint sensitivity analysis method, the computational domain is discretized into rectangular cells as in a FD grid. Figure 1 illustrates the FD 2-D grid for a lossy dielectric rectangular object, which is modeled with constitutive parameters ε_{r2} and σ_2 . The host medium is modeled with ε_{r1} and σ_1 . The vertical \mathbf{E} -field component of a 2-D TM mode is computed at the nodes of the grid. In original approach [7, 10-11], the sensitivity solver adopts the grid of the FDTD simulation. In order to compute the response Jacobians, the field at all perturbation grid points is stored and post-processed. For example, if the response derivatives with respect to ε_{r2} and σ_2 are needed, the waveforms of all nodes marked with black dots in Fig. 1(a) must be stored.

The grid of the sensitivity solver can be independent of the simulation grid because it is nothing more than a discrete means of calculating the sensitivity integral equation (17). Note that the spatial discretization defined by the step size $\Delta \chi$ can be many times larger than the

step size Δh used by the FDTD simulation. While Δh relates to Δt through the Courant stability condition, $\Delta \chi$ is limited only by the smoothness of the integrated field quantity in the perturbation region. We emphasize that a coarse grid for the sensitivity calculation does not imply in any way a possibility to use a coarse grid in the FDTD analysis. The accuracy of the sensitivity calculation depends crucially on the accuracy of the field solution and, therefore, the grid of the EM simulation must remain fine enough to ensure convergent numerical analysis.

To illustrate the coarse sensitivity grid, three different grids are shown in Fig. 1(b): the black crosses are used for the case $\Delta \chi = 2\Delta h$; the red squares for $\Delta \chi = 4\Delta h$; and the blue circles for $\Delta \chi = 8\Delta h$. We note that the number of stored field waveforms decreases as $3k^3$ in a 3-D simulation and as k^2 in a 2-D simulation when the grid is made coarser by a factor $k = \Delta \chi / \Delta h$.

The coarse sensitivity-solver grid may be applied to shape parameters as well although the savings in memory are not as dramatic since perturbation grid points exist

only at the object's interfaces instead of its whole volume. For instance, when the response gradient with respect to w is computed, the nodes where the field is saved are shown in Figs. 2(a-b). The black dots in Fig. 2(a) are the perturbation nodes for our original approach. Figure 2(b) shows the perturbation nodes for the three coarse grids: black crosses for $\Delta \chi = 2\Delta h$ (12 nodes), red squares for $\Delta \chi = 4\Delta h$ (6 nodes), and blue circles for $\Delta \chi = 8\Delta h$ (3 nodes).

Coarse grids are needed for computationally large objects, i.e., objects which are more than several Δh in size, due to the excessive memory requirements. For computationally small objects, we suggest that the sensitivity solver adopts the simulation grid, i.e. $\Delta \chi = \pm \Delta h$. In the case of computationally large objects, we investigate the limits of the factor $k = \Delta \chi / \Delta h$, below which the Jacobian computation is of acceptable accuracy. We consider 1-D, 2-D and 3-D examples and give recommendation.

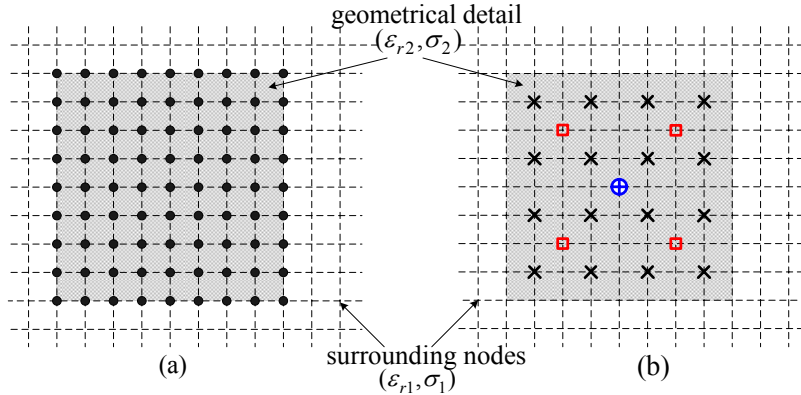


Fig. 1. Sensitivity solver grid: (a) the fine simulation grid; (b) the coarse sensitivity-analysis grids.

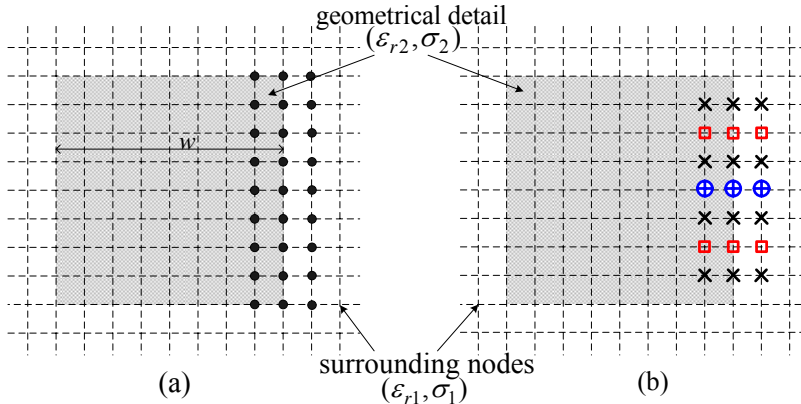


Fig. 2. Sensitivity solver grid: (a) the fine simulation grid (b) the coarse sensitivity-analysis grids.

IV. NUMERICAL RESULTS AND DISCUSSION

Our approach is verified through 1-D, 2-D and 3-D dielectric lossy inhomogeneous examples. We compute the S -parameter derivatives and the derivatives of a point-wise response function with respect to both constitutive and shape parameters for electrically large and small objects. Field analyses are carried out in the time domain with the commercial FDTD-based solvers XFDTD [12] and QW-3D [13]. Mesh convergence is checked for all examples. The convergence error formula is,

$$e = \left| \tilde{E}_\zeta^{(k+1)} - \tilde{E}_\zeta^{(k)} \right| / \left| \tilde{E}_\zeta^{(k+1)} \right|, \quad \zeta = x, y, z. \quad (23)$$

Here, the superscripts denote two consecutive mesh sizes. $\tilde{E}_\zeta^{(k+1)}$ and $\tilde{E}_\zeta^{(k)}$ are the phasors of the field solutions for two consecutive mesh sizes at the highest frequency of interest. This error is usually monitored at the ports for S -parameter analysis or at the observation points P and Q .

In all plots, the results obtained using the original approach of self-adjoint sensitivity analysis are marked as ‘FDTD-SASA’. The results obtained using coarse-grid schemes of the self-adjoint sensitivity analysis are marked as ‘ $\Delta\chi = k\Delta h$ ’, which means that the sensitivity-solver grid is k times coarser than the FDTD grid. The results estimated using the forward, central and backward finite differences are marked as ‘FFD’, ‘CFD’ and ‘BFD’, respectively. For shape parameter derivatives, the FD estimates use parameter perturbation of $1\Delta h$ unless specified otherwise in brackets in the plot’s legend. For material parameters derivatives, the amount of parameter perturbation is shown in brackets as a percentage of the nominal value. Where available, analytical results are marked as ‘Analytical’. All analyses are performed over a frequency range from 3.0 GHz to 5.0 GHz, which is the bandwidth of the excitation pulse.

A. Parallel-Plate Waveguide with an Electrically Thick Layer

We first illustrate the approach with a parallel-plate waveguide (see the insert in Fig. 3) with an electrically thick inhomogeneity (shown in shade). Both media are lossy. Uniform mesh ($\Delta h = 0.25$ mm) is used in the FDTD simulation with a mesh convergence error less than 5 %. The excitation is a modulated Gaussian pulse. It has a uniform distribution across the port conforming to a TEM plane wave.

The optimizable parameters $\mathbf{p}^T = [\varepsilon_{r2}, \sigma_2, w]$ are the constitutive parameters of the central layer. Figure 3 shows the derivative of $|S_{11}|^2$ with respect to σ_2 . It is

noted that the results obtained using all coarse schemes except the one using $\Delta\chi = 20\Delta h$, which is the Nyquist limit at 5 GHz, show good agreement with the analytical, the FDTD-SASA and the CFD results.

For electrically large objects in a 1-D problem, if the optimizable parameters are material parameters, we recommend to choose the step size of the sensitivity solver as $\Delta\chi \leq \lambda_{\min}/4$ in order to maintain good accuracy. Here, λ_{\min} is the minimum wavelength of interest in the medium of the optimized object.

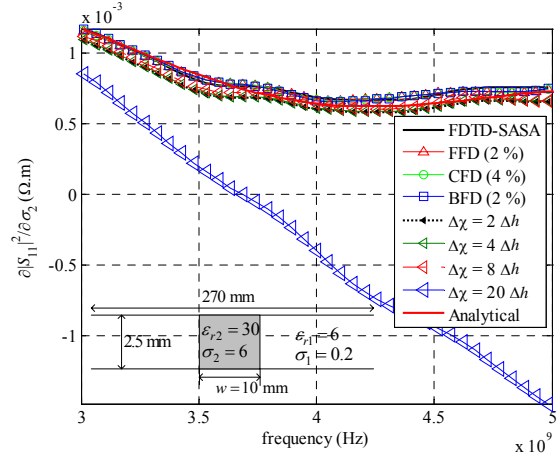


Fig. 3. Derivative of $|S_{11}|^2$ with respect to σ_2 in the 1-D example with electrically thick layer.

Figures 4 and 5 show the derivatives of the real and imaginary parts of S_{11} with respect to the shape parameter w . It is observed that all curves obtained using coarse grids except the one with $\Delta\chi = 2\Delta h$ show substantial discrepancies in comparison with the FDTD-SASA ($\Delta\chi = \Delta h$) as well as the FD curves. For 1-D problems, if the shape parameter is optimized, we recommend to choose the step size of the sensitivity solver as that of the simulation grid in order to maintain good accuracy. This is also because the memory requirements in this case are small.

B. Parallel-Plate Waveguide with a Thin Layer

A parallel-plate waveguide with an electrically thin central layer is shown in the insert of Fig. 6. Uniform mesh ($\Delta h = 0.125$ mm) with a mesh convergence error less than 4 % is used in the FDTD simulation. The excitation and the optimizable parameters are the same as in the first example.

Figure 6 shows the derivative of the real part of S_{21} with respect to ε_{r2} . It is observed that all curves obtained using different coarse-grid schemes are in good agreement. There is very small discrepancy between the

curves obtained using coarse grids and all the other curves. We conclude that for an electrically small object in a 1-D problem, the step size $\Delta\chi$ of the sensitivity solver can be chosen as large as the size of the object when derivatives with respect to material parameters are computed.

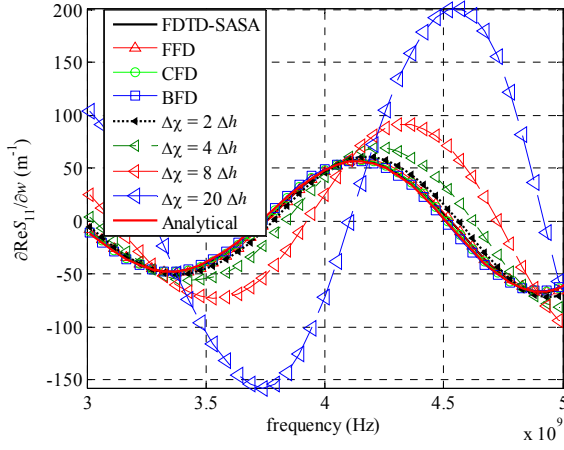


Fig. 4. Derivative of $\text{Re}(S_{11})$ with respect to w in the 1-D example with electrically thick layer.

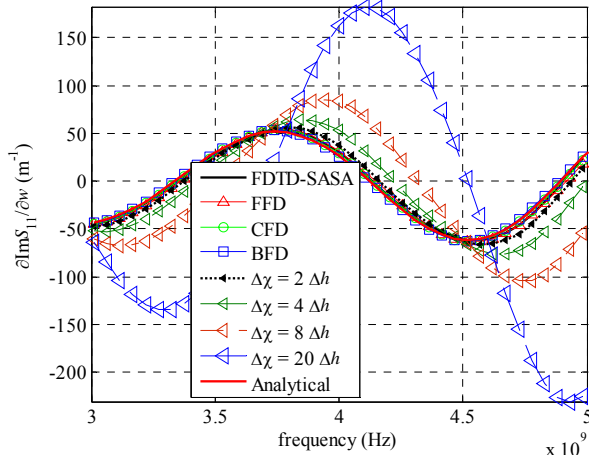


Fig. 5. Derivative of $\text{Im}(S_{11})$ with respect to w in the 1-D example with electrically thick layer.

C. Electrically Large Object in a Lossy Medium

Figure 7(a) shows a 2-D structure with an electrically large object immersed in a host medium. Both the host medium and the object are lossy. Uniform mesh ($\Delta h = 0.25$ mm) with a mesh convergence error below 4 % is used. We use the same excitation waveform as in the above examples.

The design parameters are $\mathbf{p}^T = [\varepsilon_{r2}, \sigma_2, w]$. We use the normalized point-wise response function F_{PQ} in

equation (13). In Fig. 7(a), Q is the excitation point while P is the observation point. The sensitivity of $|F_{QQ}|$ with respect to ε_{r2} and the sensitivity of $|F_{PQ}|$ with respect to w are plotted in Fig. 8 and 9, respectively. We notice that the step size of sensitivity solver can be 8 times coarser than that of the FDTD simulation. A sensitivity-grid cell size of $\Delta\chi = 16\Delta h$ corresponds to the Nyquist limit at 5 GHz for the medium of the obstacle and the respective curves show significant departure from all other results. For electrically large object in a 2-D problem, we recommend to choose the step size of the sensitivity solver as $\Delta\chi \leq \lambda_{\min}/4$ in order to maintain good accuracy.

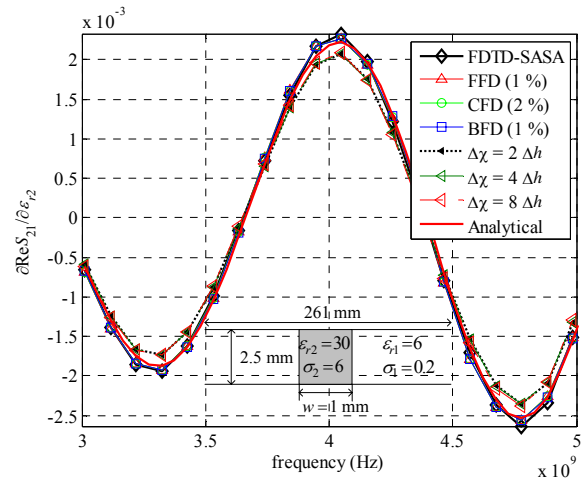


Fig. 6. Derivative of $\text{Re}(S_{21})$ with respect to ε_{r2} in the 1-D example with electrically thin layer.

D. Electrically Small Object in a Lossy Medium

Figure 7(b) shows a 2-D structure with an electrically small inhomogeneity in a host medium. Both the host medium and the inhomogeneity are lossy. A uniform mesh ($\Delta h = 0.125$ mm) with a mesh convergence error below 3 % is used. The excitation, design parameters, and the response functions are the same as those in the example in subsection C.

In Fig. 7(b), Q is the excitation point while P is the observation point. The sensitivities of $|F_{PQ}|$ with respect to σ_2 and w are plotted in Fig. 10 and 11, respectively. We notice that the step size of the sensitivity solver needs to be the same as the step size of the FDTD simulation in order to achieve good accuracy. For electrically small objects in 2-D problems, we recommend to choose the step size of the sensitivity solver as that of the FDTD simulation for both shape and material parameters in order to maintain good accuracy.

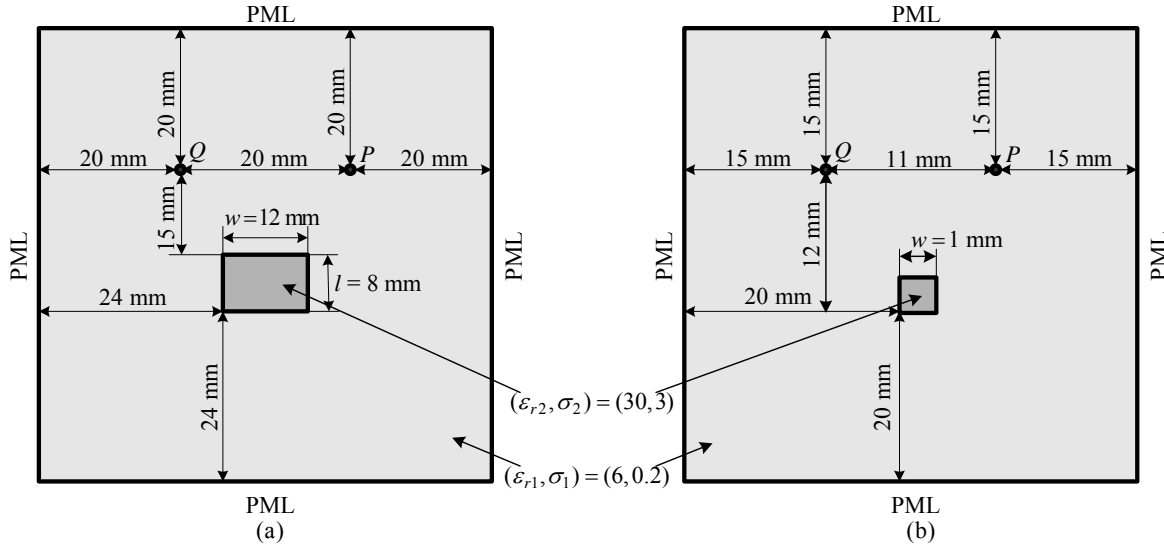


Fig. 7. Geometry of 2-D examples: (a) electrical large and (b) electrical small objects in lossy medium.

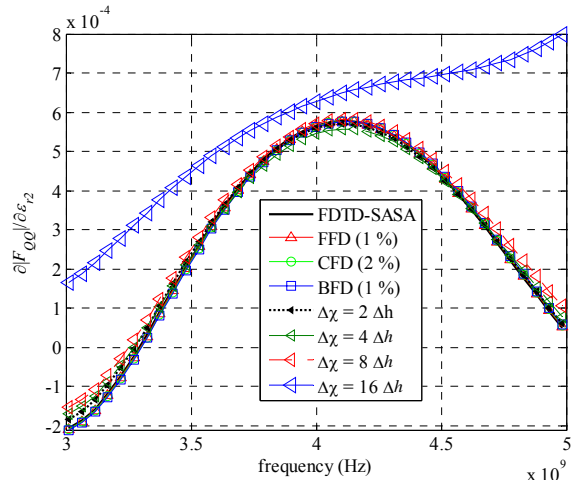


Fig. 8. Derivative of $|F_{QQ}|$ with respect to ϵ_{r2} in the 2-D example with a large object.

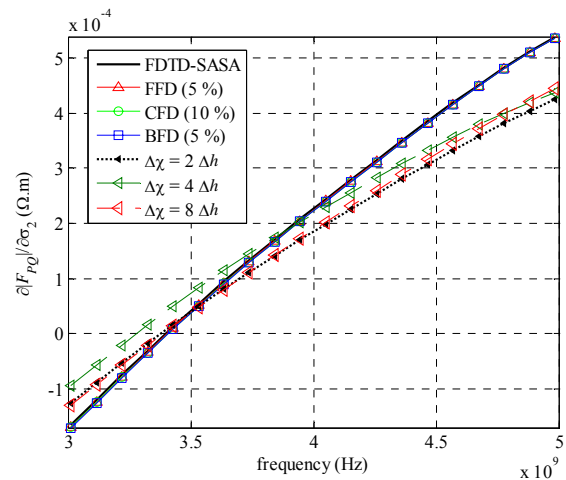


Fig. 10. Derivative of $|F_{PQ}|$ with respect to σ_2 in the 2-D example with a small object.

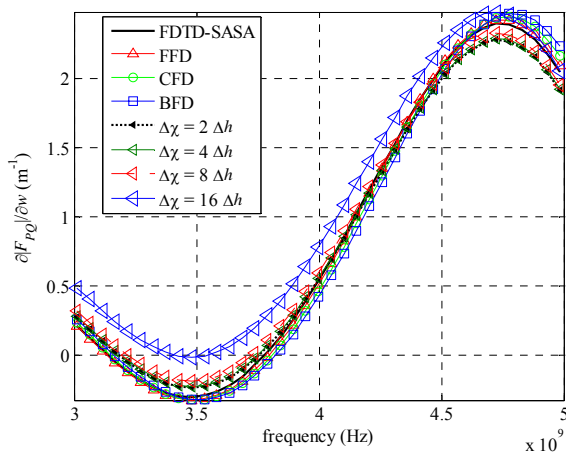


Fig. 9. Derivative of $|F_{PQ}|$ with respect to w in the 2-D example with a large object.

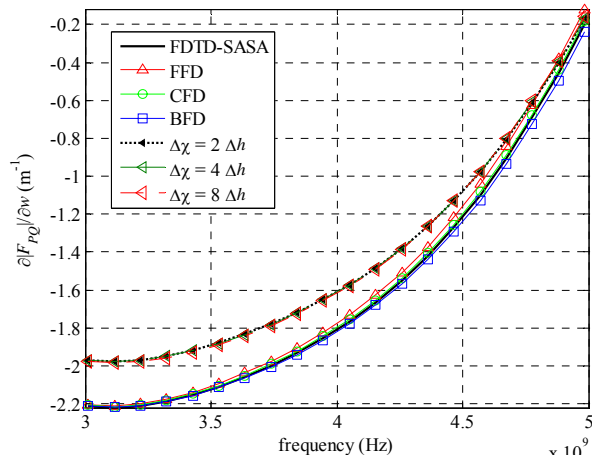


Fig. 11. Derivative of $|F_{PQ}|$ with respect to w in the 2-D example with a small object.

V. CONCLUSIONS

We propose a coarse-grid approach for the efficient computation of response Jacobians using the self-adjoint sensitivity analysis method. The sensitivity-analysis grid can be many times coarser than the grid used by the EM simulation. We emphasize that the accuracy of the sensitivity result is dependent on the accuracy of the field solution and, therefore, the grid of the EM simulation must remain fine enough to ensure convergent solution. Yet, the sensitivity grid can be as coarse as a quarter wavelength for the highest frequency of interest. This is because it is nothing more than a discrete means of calculating the sensitivity integral. It is limited only by the requirement that the local field solution is a sufficiently smooth function of space at the given frequency.

The coarse-grid approach reduces the memory requirements drastically. It is especially useful in the case of electrically large regions whose permittivity or conductivity distribution is being optimized, since the memory requirement of our original self-adjoint approach, which uses the FDTD simulation grid directly, may become excessive. The coarse-grid Jacobian computations are verified through 1-D, 2-D and 3-D examples. We find that they maintain very good accuracy as long as the step size of the sensitivity solver is below the Nyquist limit. Recommendations about the step size of the sensitivity solver are given for both electrically large and small objects.

Our new grid scheme is independent of the simulation grid and is simple to implement. The approach can be realized as standalone software to compute response Jacobians, which can be used in gradient-based computer-aided design and inverse-problem solutions. Applications focus on lossy dielectric media as those used to model high-frequency problems arising in biomedical applications of microwave imaging.

REFERENCES

- [1] Y. Chung, C. Cheon, I. Park, and S. Hann, "Optimal shape design of microwave device using FDTD and design sensitivity analysis," *IEEE Trans. Microw. Theory Tech.*, vol. 48, no. 12, pp. 2289-2296, Dec. 2000.
- [2] Y. Chung, J. Ryu, C. Cheon, I. Park, and S. Hahn, "Optimal design method for microwave device using time domain method and design sensitivity analysis-Part I: FETD case," *IEEE Trans. Magn.*, vol. 37, no. 9, pp. 3289-3293, Sep. 2001.
- [3] Y. Chung, J. Ryu, C. Cheon, I. Park, and S. Hahn, "Optimal design method for microwave device using time domain method and design sensitivity analysis-Part II: FDTD case," *IEEE Trans. Magn.*, vol. 37, no. 9, pp. 3255-3259, Sep. 2001.
- [4] N. K. Nikolova, J. W. Bandler, and M. H. Bakr, "Adjoint techniques for sensitivity analysis in high-frequency structure CAD," *IEEE Trans. Microw. Theory Tech.*, vol. 52, no. 1, pp. 403-419, Jan. 2004.
- [5] Q. Fang, P. M. Meaney, S. D. Geimer, K. D. Paulsen, and A. V. Streltsov, "Microwave image reconstruction from 3-D fields coupled to 2-D parameter estimation," *IEEE Trans. Med. Imag.*, vol. 23, pp. 475-484, Apr. 2004.
- [6] Y. Song and N. K. Nikolova, "Sensitivity analysis of electrically small objects in lossy inhomogeneous structures," *IEEE AP-S Int. Symp.*, pp. 4453-4456, June 2006.
- [7] N. K. Nikolova, Ying Li, Yan Li, and M. H. Bakr, "Sensitivity analysis of scattering parameters with electromagnetic time-domain simulators," *IEEE Trans. Microw. Theory Tech.*, vol. 54, pp. 1589-1610, April 2006.
- [8] N. K. Nikolova, H. W. Tam, and M. H. Bakr, "Sensitivity analysis with the FDTD method on structured grids," *IEEE Trans. Microw. Theory Tech.*, no. 52, pp. 1207-1216, 2004.
- [9] M. H. Bakr and N. K. Nikolova, "An adjoint variable method for time domain TLM with fixed structured grids," *IEEE Trans. Microw. Theory Tech.*, vol. 52, pp. 554-559, Feb. 2004.
- [10] Yang Li, Yan Li, N. K. Nikolova, and M. H. Bakr, "Time domain sensitivity analysis of lossy dielectric structures," *Frontiers of Applied Computation Electromagnetics (FACE) 2006 CDROM* (Victoria, BC), June 2006.
- [11] Y. Song, Y. Li, N. K. Nikolova and M. H. Bakr, "Self-adjoint sensitivity analysis of lossy dielectric structures with electromagnetic time-domain simulators," *Int. J. of Numerical Modelling: Electronic Networks, Devices and Fields* (accepted).
- [12] XFDTD v. 6.2, *Reference Manual*, Remcom, 2004, <http://www.recom.com/xfdfd6/>.
- [13] QuickWave-3D v. 6.0, *Reference Manual*, QWED, 2006, <http://www.qwed.com.pl/index.htm>.
- [14] N. Marcuvitz, *Waveguide Handbook*, Chapter 2, London, UK: Peter Peregrinus Ltd., 1993 reprint.

[15]C. A. Balanis, *Antenna Theory: Analysis and Design*, 3rd ed., New Jersey, USA: John Willey & Sons, Inc., 2005



Yunpeng Song received the M. Sc. Degree in electrical engineering from Concordia University, Montreal, Canada, in 2005, and is currently working toward the Ph. D degree in electrical engineering at McMaster University, Hamilton, ON, Canada. His research interests include computational electromagnetics, inverse-scattering problems, optimization methods, computer-aided analysis and design in microwave engineering and antennas.



Natalia K. Nikolova received the Dipl. Eng. degree from the Technical University of Varna, Bulgaria, in 1989, and the Ph.D. degree from the University of Electro-Communications, Tokyo, Japan, in 1997. From 1998 to 1999, she held a Postdoctoral Fellowship of the Natural Sciences and Engineering Research Council of Canada (NSERC), during which time she was initially with the Microwave and Electromagnetics Laboratory, DalTech, Dalhousie University, Halifax, Canada, and, later, for a year, with the Simulation Optimization Systems Research Laboratory, McMaster University, Hamilton, ON, Canada. In July 1999, she joined the Department of Electrical and Computer Engineering, McMaster University, where she is currently an Associate Professor. Her research interests include theoretical and computational electromagnetism, inverse problems and microwave imaging, as well as CAD methods for high-frequency structures and antennas. Prof. Nikolova was the recipient of a University Faculty Award of NSERC from 2000 to 2005. She is a senior member of the IEEE and a member of the Applied Computational Electromagnetics Society (ACES) and the International Union of Radio Science (URSI). Prof. Nikolova was the representative of Commission D in the Canadian National Committee of URSI from 2002 till 2007. She is currently a member of the ACES Board of Directors. She is a registered professional engineer in the province of Ontario, Canada.



Mohamed H. Bakr received a B.Sc. degree in Electronics and Communications Engineering from Cairo University, Egypt in 1992 with distinction (honors). In June 1996, he received a Master's degree in Engineering Mathematics from Cairo University. In 1997, he was a student intern with Optimization Systems Associates (OSA), Inc. From 1998 to 2000, he worked as a research assistant with the Simulation Optimization Systems (SOS) research laboratory, McMaster University, Hamilton, Ontario, Canada. He earned the Ph.D. degree in September 2000 from the Department of Electrical and Computer Engineering, McMaster University. In November 2000, he joined the Computational Electromagnetics Research Laboratory (CERL), University of Victoria, Victoria, Canada as an NSERC Post Doctoral Fellow. His research areas of interest include optimization methods, computer-aided design and modeling of microwave and photonic circuits, neural network applications, smart analysis of microwave circuits, efficient optimization using time/frequency domain methods, and bio-electromagnetism. He is currently an associate professor with the Department of Electrical and Computer Engineering, McMaster University. Dr. Bakr was a recipient of a Premier's Research Excellence Award (PREA) from the province of Ontario, Canada, in 2003.